Electronic Supplementary Information

A facile design of thio-perylenediimides with controllable fluorescent, photodynamic and photothermal effects towards cancer theranostics

Chang Liu, [a] Chendong Ji, [a] Zongyang Fan, [a] Ruihao Ma [a] and Meizhen Yin *[a]

a State Key Laboratory of Chemical Resource Engineering, Beijing Laboratory of Biomedical Materials, Beijing University of Chemical Technology, Beijing 100029, China.

Table of contents

Experimental Procedures

1.1 Materials and Methods

1.1.1 Materials

1,6,7,12-Tetrachloroperylene tetracarboxylic acid dianhydride (Energy Chemical, 95%), Octylamine (Alfa, 98%), 4-tert-Butylphenol (TCI, 98%), N-Methyl-2-pyrrolidinone (Energy Chemical, 99%), Lawesson's Reagent (TCI, 95%). Organic solvent: Dichloromethane, n-Hexane, Propanoic Acid, dimethylbenzene (Beijing Chemical Works, Analytically pure). Deionized (DI) water (18.2 MΩ•cm resistivity at 25 ^{o}C) was prepared through a Millipore Milli-Q purification system. Column chromatography was performed on silica gel (Davisil Grade 643, Aladdin). Cell counting kit (CCK-8), Dulbecco's Modified Eagle's Medium (DMEM), calcein-AM and propidium iodide (PI) chromophore stuff were purchased from Dojindo Laboratories (Japan).

1.1.2 Morphology and Characterization.

The UV-vis-NIR absorption spectrum of PDI-O~4S was recorded on a spectrophotometer (UV-2450, SHIMADZU). The fluorescence emission spectrum of PDI-O~4S was recorded on a spectrophotometer (Horiba, FluoroMax-4 NIR). Transmission electron microscopy (TEM, HT-7700, Hitachi, Japan) determined the morphology of nanoparticles. Particle Size Analyzer (ZEN3600, Malvern) determined the size and zeta potentials of nanoparticles in water. The infrared (IR) imaging and photothermal heating curves were recorded by a Fluke (Ti400) thermal imaging camera. PDI-O~4S NPs was Diode Laser Cell level fluorescence imaging was measured via EVOS™ FL Imaging System. Photoacoustic imaging of PDI-4S NPs was measured via Multispectral Optoacoustic Tomography (MSOT) INVISIO-256 system (iThera Medical) using a phantom. Nuclear magnetic resonance (^{1}H and ^{13}C NMR) spectra were recorded on a Bruker 400 spectrometer at room temperature. Matrix-assisted laser desorption/ionization time-of-flight mass spectrometry (MALDI-TOF MS) was measured with Kratos PC Axima CFRplus V2.4.1.

1.2 Synthesis of PDI-O~S4

1.2.1 Synthesis of P1

The 1,6,7,12-Tetrachloroperylene tetracarboxylic acid dianhydride compound (4Cl-PDA, 2 g, 3.77 mmol) and octylamine (2.9 g, 22.64 mmol) were added to a reaction flask, and propionic acid (150 mL) was added as a solvent. They were placed in an oil bath with constant temperature and were refluxed for 48 h. After cooling to room temperature, the mixture was dropped into KOH aqueous solution (1 L) in batches, and the pH was adjusted to neutral. After filtration, it was dried in an oven at 50 ^{o}C, and the orange solid was obtained as the raw product. Using dichloromethane/hexane (v/v = 1:1) as eluent, the raw product was purified by silica gel column chromatography resulting in P1 (1.9 g, 67%) as red solid. ^{1}H NMR (400 MHz, $CDCl_3$) δ 8.68 (d, J = 12.5 Hz, 4H), 4.22 (dd, J = 14.8, 7.2 Hz, 4H), 1.74 (dt, J = 15.1, 7.5 Hz, 4H), 1.35 – 1.21 (m, 20H), 0.92 – 0.86 (m, 6H).

1.2.2 Synthesis of PDI-O

N,N'-bis(n-octyl)-1,6,7,12-Tetrachloroperylene-3,4:9,10-bis(dicarboximide) compound (P1, 1.5 g, 1.99 mmol), 4-tert-butyl phenol (2.2 g, 15.92 mmol) and ground potassium carbonate (2.2 g, 15.92 mmol) were added to a reaction flask with NMP (150 mL) as the solvent. It was placed in an oil bath with constant temperature at 90°C and reacted for 10 h. After cooling to room temperature, the mixture was added to saturated salt solution (1L), followed by was washed with water and drying under vacuum. The dark red solid was obtained as the raw product. The product was next chromatographed on silica gel eluting with dichloromethane as eluent and result in PDI-O (2.14 g, 89%) as dark red solid. ^{1}H NMR (400 MHz, $CDCl_3$) δ 8.22 (s, 4H), 7.25 – 7.18 (m, 8H), 6.86 – 6.80 (m, 8H), 4.14 – 4.06 (m, 4H), 1.66 (s, 4H), 1.41 – 1.16 (m, 56H), 0.84 (t, J = 6.9 Hz, 6H). PDI-O: ^{13}C NMR (101 MHz, $CDCl_3$) δ 163.44, 155.96, 152.91, 147.29, 132.90, 126.66, 122.50, 120.50, 119.89, 119.41, 40.68, 34.38, 31.79, 31.47, 29.71, 29.23, 28.12, 27.13, 22.61, 14.06. MS (MALDI-TOF), m/z: Calculated for $C_{80}H_{90}N_2O_8$+: 1206.67, found 1207.7.

1.2.3 Synthesis of PDI-O~4S

A 4-tert-butyl phenol-substituted perylene imide compound (PDI-O, 0.5 g, 0.41 mmol) and Lawson's reagent (0.669 g, 1.65 mmol) were added to a microwave reaction tube with xylene (5 mL) as a solvent. Next, it was placed in a 150 W microwave reactor at 103°C for 20 min. After cooling to room temperature, the mixture was added with 45 mL methanol, and the solvent was removed through azeotropic distillation. Then the product was dissolved in dichloromethane and extracted three times with saturated salt solution. After the water was removed by anhydrous sodium sulfate, the solvent was removed by rotary evaporation to obtain the blue-green solid as the raw product. The product was next chromatographed on silica gel eluting with dichloromethane/hexane (V/V = 2/5) as eluent and result in PDI-1S (50 mg, 10%) as blue solid, PDI-2S (76 mg, 15%) as lake blue solid, and PDI-3S (97 mg, 19%) as green solid and PDI-4S (125 mg, 24%) as dark brown solid.

PDI-1S: ^{1}H NMR (400 MHz, $CDCl_3$) δ 8.69 – 8.64 (m, 1H), 8.26 – 8.17 (m, 3H), 7.26 – 7.20 (m, 8H), 6.91 – 6.75 (m, 8H), 4.66 (d, J = 7.9 Hz, 2H), 4.09 (dd, J = 7.8, 7.1 Hz, 2H), 1.72-1.59 (m, 4H), 1.36 – 1.26 (m, 56H), 0.88 – 0.83 (m, 4H). ^{13}C NMR (101 MHz, $CDCl_3$) δ 191.45, 162.38, 159.72, 155.10, 154.32, 152.28, 151.81, 146.30, 145.90, 131.85, 131.47, 126.42, 125.57, 124.39, 121.59, 119.56, 119.03, 118.74, 118.36, 117.77, 117.04, 46.44, 39.66, 33.34, 30.77, 30.44, 28.68, 28.20, 27.09, 26.06, 25.62, 21.59, 13.04. MS (MALDI-TOF), m/z: Calculated for $C_{80}H_{90}N_2O_7S+$: 1222.65, found 1223.5.

PDI-2S: ^{1}H NMR (400 MHz, $CDCl_3$) δ 8.66 (d, J = 9.7 Hz, 2H), 8.29 – 8.15 (m, 2H), 7.25 (dd, J = 4.7, 4.0 Hz, 8H), 6.93 – 6.76 (m, 8H), 4.75 – 4.58 (m, 4H), 1.72 (m, 4H), 1.36 – 1.27 (m, 56H), 0.88 (d, J = 6.7 Hz, 6H). ^{13}C NMR (101 MHz, $CDCl_3$) δ 191.41, 159.72, 155.27, 154.48, 152.22, 151.73, 146.37 (s), 145.95, 131.46, 126.45, 125.59, 124.27, 121.76, 119.60, 118.88, 118.41, 117.82, 116.99, 46.45 (s), 33.35, 30.78, 30.45, 28.69, 28.19, 26.02, 25.63, 21.60, 13.05. MS (MALDI-TOF), m/z: Calculated for $C_{80}H_{90}N_2O_6S_2+$: 1238.62, found 1239.5.

PDI-3S: ^{1}H NMR (400 MHz, $CDCl_3$) δ 8.61 (d, J = 4.6 Hz, 1H), 8.54 (d, J = 10.0 Hz, 2H), 8.18 (s, 1H), 7.24 (d, J = 4.0 Hz, 8H), 6.90 – 6.74 (m, 8H), 5.35 (d, J = 4.4 Hz, 2H), 4.63 (d, J = 8.1 Hz, 2H), 1.71 (m, 4H), 1.32 – 1.25 (m, 56H), 0.86 (d, J = 4.3 Hz, 6H). ^{13}C NMR (101 MHz, $CDCl_3$) δ 190.96, 187.35, 159.70, 155.38, 154.76, 154.56, 152.13, 151.67, 146.40, 145.99, 131.44, 128.15, 125.58, 124.84, 124.15, 121.78, 119.60, 118.45, 117.87, 116.95, 114.14, 53.96, 46.53, 33.34, 30.78, 30.45, 28.15, 26.01, 25.66, 24.35, 21.61, 13.06. MS (MALDI-TOF), m/z: Calculated for $C_{80}H_{90}N_2O_5S_3$+: 1254.60, found 1255.6.

PDI-4S: ^{1}H NMR (400 MHz, $CDCl_3$) δ 8.51 (s, 4H), 7.25 (d, J = 2.2 Hz, 8H), 6.82 (d, J = 8.7 Hz, 8H), 5.28 – 5.21 (m, 4H), 1.66 (m, 4H), 1.31-1.25 (m, 56H), 0.87 – 0.82 (m, 6H). ^{13}C NMR (101 MHz, $CDCl_3$) δ 187.25, 154.91, 152.07, 146.03, 131.05, 128.12, 125.51, 124.70, 119.70, 117.93, 114.11, 54.14, 33.35, 30.79, 30.45, 28.15, 25.67, 24.36, 21.62, 13.08. MS (MALDI-TOF), m/z: Calculated for $C_{80}H_{90}N_2O_4S_4$+: 1270.58, found 1271.6.

1.3 Preparation of PDI-O~4S NPs

To prepare water-soluble PDI-O~4S NPs, triblock copolymers F127 (15 mg) and thionated PDIs (1 mg) were dissolved in 1,4 dioxane (3 mL), and then the organic mixture was slowly added to the deionized water (3 mL) at a constant rate. After stirring for 2 h, the solution was dialyzed in deionized water for 48 h using the cellulose membrane (cutoff molecular weight of 3500 Da). PDI-O~4S nanoparticles (PDI-O NPs, PDI-1S NPs, PDI-2S NPs, PDI-3S NPs and PDI-4S NPs) can be obtained by dissolving the product in deionized water and stirring at a steady and uniform speed for 2h.

1.4 Detection of singlet oxygen ($^1O_2$) generation of thionated PDIs and PDI-1S~4S NPs

The singlet oxygen generation of thionated PDIs in organic solvent and PDI-1S~4S NPs in aqueous solution was tested by using Kraljic procedure. The thionated PDIs molecule and singlet oxygen detection agent DPBF were dissolved in dichloromethane. The laser power was fixed at 5 mW cm^{-2}. PDI-O was irradaited by 550 nm green light for 10 s every time, PDI-1S was irradiated by 620 nm red light for 5 s every time, PDI-2S was irradiated by 650 nm red laser for 10 s and PDI-3S was irradiated by 700 nm NIR light for 10 s, and PDI-4S was irradiated by 770 nm NIR light for 10 s. After each irradiation, the absorbance was monitored by UV-vis spectrophotometer. Singlet oxygen can bleach DPBF and reduce its absorbance at 417 nm. PDI-1S~4S NPs and water-soluble singlet oxygen detection agent water soluable DPBF were added in aqueous solution. The PDI-1S NPs were used 660 nm laser irradiation for 5 s with laser power of 15 mW cm^{-2}, PDI-2S NPs were used 660 nm laser irradiation for 60 s with laser power of 15 mW cm^{-2}, and PDI-3S NPs was irradiated by 660 nm laser for 60 s with laser power of 200 mW cm^{-2}. The PDI-4S NPs was irradiated by 808 nm laser for 60 s with laser power of 200 mW cm^{-2}. After each irradiation, the absorbance was monitored by UV-vis spectrophotometer. Singlet oxygen can bleach DPBF and reduce its absorbance at 417 nm. The following equation was used,[1] where m is the slope of the absorption change of DPBF at 417 nm against the irradiation time. F is the absorption correction factor, which is given as $F = 1\text{-}10^{-OD}$. P is the absorbed photonic flux:

$$\Phi(\text{PS})=\Phi(\text{MB}) \times \frac{\text{m(PS)}}{\text{m(MB)}} \times \frac{\text{F(MB)}}{\text{F(PS)}} \times \frac{\text{P(MB)}}{\text{P(PS)}}$$

1.5 Computational details

TD-DFT calculations were conducted on Gaussian 09 program. Moreover, exciton energies in singlet (Sn) and triplet states (Tn) were estimated through a TD-DFT method at the TD-B3LYP/6-31+G (d, p) level.[2] All the natural transition orbitals (NTO) analysis were evaluated by Multiwfn program based on TD-DFT results using Gaussian 09 package. Spin-orbital coupling (SOC) matrix elements were investigated by ORCA program (version 4.1) based on the TD-DFT results.[3-5] The formation of $^1O_2$ was directly proportional to ISC rate constant (k_{ISC}).[6] Furthermore, k_{ISC} was relative with the singlet-triplet energy gap (ΔE_{ST}) and the SOC constants, ($<S_n|H_{\text{SO}}|T_m>$), and can be described using the relevant equation.[7]

$$k_{\text{ISC}} \propto \frac{\langle \text{S}_n | H_{\text{SO}} | \text{T}_m \rangle^2}{\left(\Delta E_{\text{S}_n-\text{T}_\text{m}}\right)^2}$$

1.6 Photothermal conversion efficiency of PDI-1S~4S NPs in aqueous solution

The 1.0 mL PDI-1S~4S NPs aqueous solution was placed in a quartz cuvette with OD of 1 at the main excitation peak. PDI-1S NPs, PDI-2S NPs and PDI-3S NPs were irradiated at 1W cm^{-2} by 660 nm laser for about 15 min. PDI-4S NPs was irradiated with an 808 nm laser at 1W cm^{-2} for about 15 minutes. Pure water was used as control group. When the increased temperature reaches a stable state, the laser is turned off to allow the PDI-1S~4S NPs aqueous solution to cool naturally. Throughout the process, the temperature was recorded by a thermal imaging camera. The photothermal conversion efficiency (η) was calculated according to reported work.[8]

$$\eta = \frac{hA\Delta T_{max} - Q_s}{I(1-10^{-A_{660}})}$$

where h is the heat transfer coefficient, A is the surface area of the container, T_{max} is the maximum steady-state temperature, T_{sur} is the ambient temperature of the environment, Q_s is the heat dissipation of solvent (water) measured by a power meter (407A, Spectra-Physics), I is the incident laser power (1 W cm^{-2}), and A_{660} is the absorbance of the PDI-1S NPs, PDI-2S NPs and PDI-3S NPs at 660 nm. and A_{808} is the absorbance of the PDI-4S NPs at 808 nm. hA was calculated by the following equation:

$$hA = \frac{\sum m_i C_i}{\tau_s}$$

where m and C_i are the mass (1 g) and heat capacity (4.2 J/g) of water, respectively. τs is the sample system time constant calculated by the following equation:

$$\tau_s = -\frac{T}{\ln\theta}$$

where T represents time. θ is the dimensionless driving force defined as $(T-T_{sur})/(T_{max}-T_{sur})$.

1.7 Photoacoustic (PA) imaging in plantation

Control group (DI water) and different concentrations of PDI-O~4S NPs solution (60 μM) were loaded into the plantation. The PA signals were acquired on the multispectral optical tomography system (MSOT in Vision 256, iThera8 Medical, Germany) under excitation wavelengths (680-900 nm). The concentration and signal intensity were fitted linearly.

1.8 The assessment of photothermal stability

Aqueous solution (1.0 mL) of PDI-4S NPs (50 μM) was placed in a quartz cuvette and irradiated with 808 nm laser light at 1 W cm^{-2} for 10 min, followed by the PDI-4S NPs aqueous solution allowed to cool after laser light shut off. When the temperature dropped to near room temperature, the aqueous solution of PDI-4S NPs was irradiated with 808 nm laser light at 1 W cm^{-2} for 10 min again. Repeat the above operation three times. An infrared-thermal camera was utilized to record the temperature of the solution every 20 s.

1.9 Cell culture

Murine mammary carcinoma cells (4T1) were incubated in DMEM medium containing 10% FBS and 1% antibiotics (penicillin-streptomycin). Cells were cultured at 37 °C in a humidified atmosphere containing 21% O_2 and 5% CO_2.

1.10 Cytotoxicity tests of PDI-1S~4S NPs

4T1 cells were seeded into 96-well plates at a density of 5 × 10^3 cells per well. After incubation for 12 h, the cells were co-incubated with PDI-O NPs, PDI-1S NPs, PDI-2S NPs, PDI-3S NPs or PDI-4S NPs at different concentrations of 100 μM, 50 μM, 20 μM, 10 μM, 5 μM, 2 μM, 1 μM and 0 μM. 4T1 cells were co-incubated with PDI-1S NPs, PDI-2S NPs, PDI-3S NPs or PDI-4S NPs for 24 h and 48 h, respectively. After incubation, the cell viability was tested by CCK-8. CCK-8 (10 μL) was added into each well. After incubation for 4 h, the absorbance (450 nm) was measured using a microplate reader. The cell viabilities (%) were calculated as follows: (OD tested well - OD medium control) / (OD untreated well - OD medium control) × 100%.

1.11 PDI-O NPs fluorescence imaging in vitro

4T1 cells were seeded into 96-well plates with a density of 5×10^3 cells per well. After overnight culture, 4T1 cells were incubated with PDI-O NPs (5 μM) for 6h, and then were washed with PBS for 3 times. Red fluorescence signal was detected by fluorescence microscope.

1.12 Detection of the cellular reactive oxygen species (ROS)

The 4T1 cells were seeded in 96-well plates with a density of 5×10^3 cells per well and cultured for 12 h. After further incubated with PDI-1S NPs, PDI-2S NPs, PDI-3S NPs or PDI-4S NPs (10 μM) for 12 h, respectively, the cells were irradiated by laser light (660 nm or 808 nm, 100 mW cm^{-2}) for 5 min. The nanoparticles-treated cells without irradiation, and the irradiation-treated cells without nanoparticles were acted as the controls. The cells were washed with PBS and incubated with DCFH-DA (5 μM, $\lambda ex = 473$ nm, $\lambda em = 490\text{-}590$ nm) for 30 min, and inspected by fluorescence microscopy.

1.13 Phototherapy of PDI-1S~4S NPs in vitro

4T1 cells were seeded into 96-well plates at a density of 5×10^3 cells per well. In order to detect the phototherapeutic effect of PDI-1S NPs, PDI-2S NPs, PDI-3S NPs or PDI-

4S NPs *in vitro*, 4T1 cells were co-incubated with PDI-1S NPs, PDI-2S NPs, PDI-3S NPs or PDI-4S NPs with different concentrations for 12 h. Then, a 660 nm or 808 nm NIR laser with a power of 0.75 W cm^{-2} was irradiated for 5 min. After co-incubation for 6 h, CCK-8 (10 μL) was added to each well. After incubation for 4 h, the absorbance at 450nm was measured with a microplate reader, and the cell viability was calculated.

1.14 Staining of dead and living cells

4T1 cells were seeded into 96-well plates with a density of 5 × 10^3 in a well and were incubated overnight at 37 °C. The cells were co-incubated with PDI-1S NPs, PDI-2S NPs, PDI-3S NPs or PDI-4S NPs (20 μM) for 12 h. Cells were divided into two groups, one group of the cells was irradiated at 660 nm or 808 nm laser light for 5 mins with a power intensity of 0.75 W cm^{-2}. Another group was the cells without laser irradiation. Cells were co-incubated with Calcein-AM (0.2 μM) and PI solutions (0.5 μM) in PBS buffer solution (0.1 mL per well) for 20 mins at 37 °C with 5% CO_2. Cells in 96-well plates were washed with PBS three times and inspected by fluorescence microscopy.

Supplementary Data

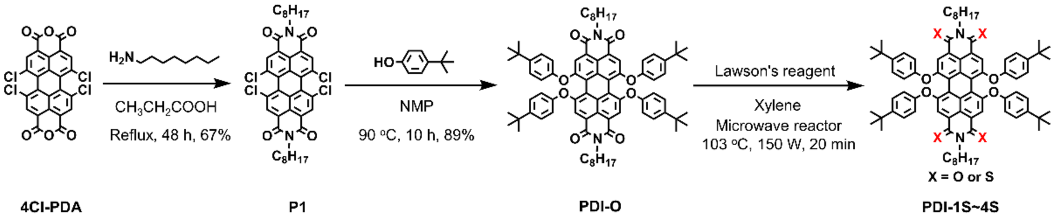

Fig. S1. The synthetic route for thionated PDIs. NMP = 1-Methyl-2-pyrrolidinone.

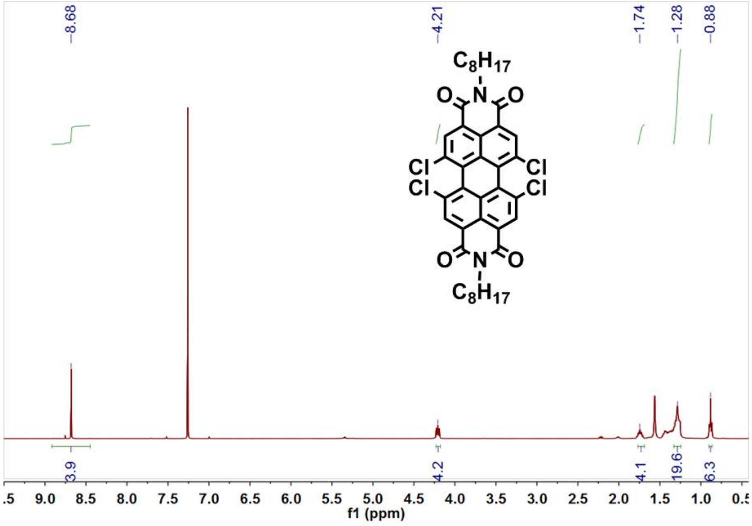

Fig. S2. ^{1}H NMR spectrum of P1.

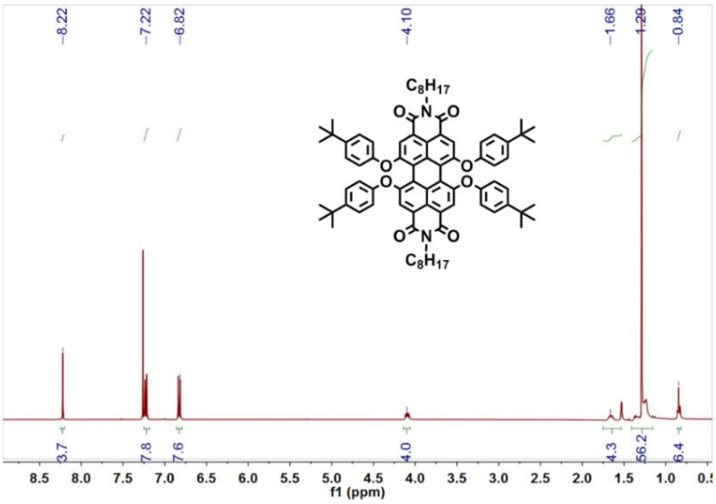

Fig. S3. ^{1}H NMR spectrum of PDI-O.

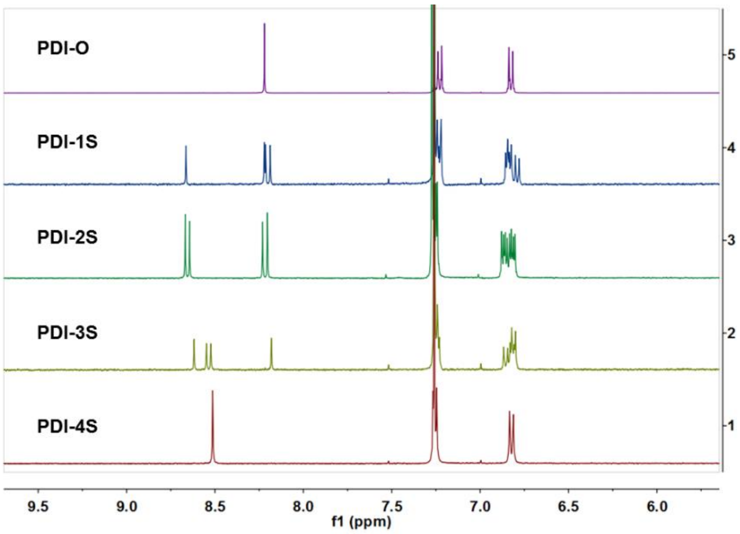

Fig. S4. ^{1}H NMR spectrum of PDI-O~4S.

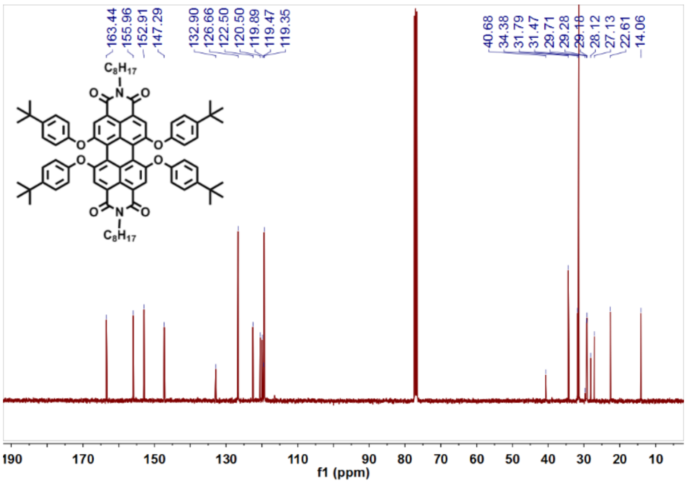

Fig. S5. ^{13}C NMR spectrum of PDI-O.

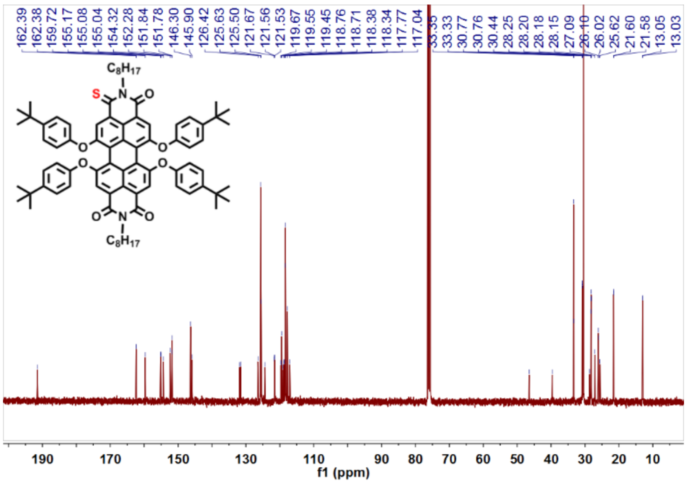

Fig. S6. ^{13}C NMR spectrum of PDI-1S.

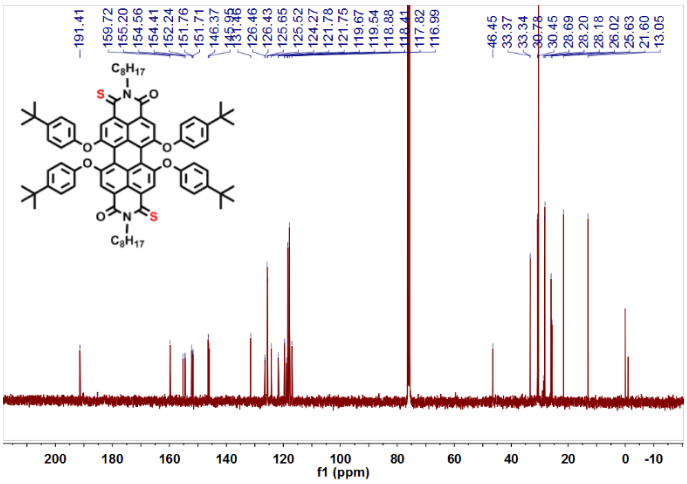

Fig. S7. ^{13}C NMR spectrum of PDI-2S.

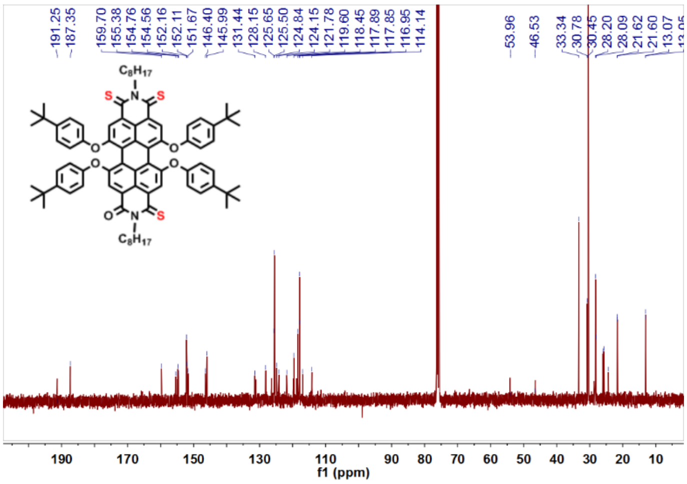

Fig. S8. ^{13}C NMR spectrum of PDI-3S.

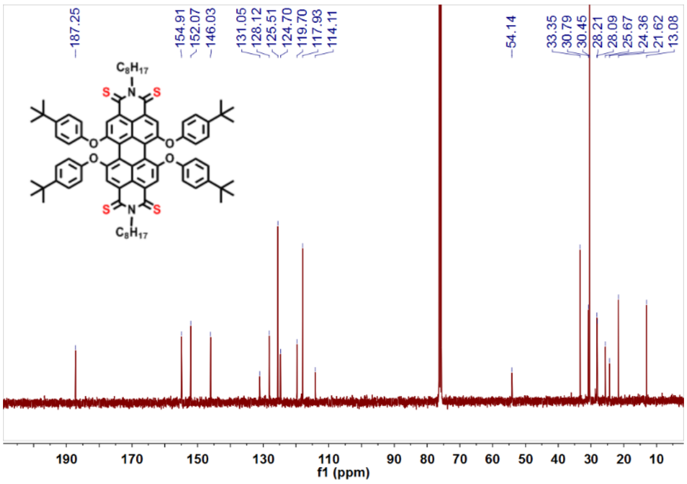

Fig. S9. ^{13}C NMR spectrum of PDI-4S.

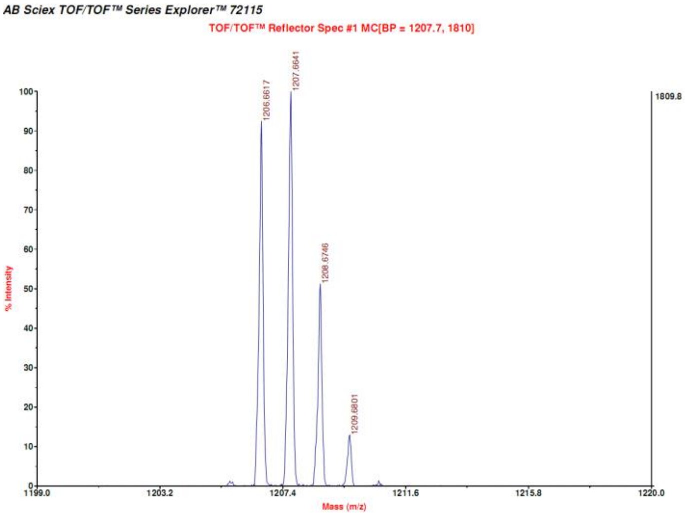

Fig. S10. MS (MALDI-TOF) mass spectrum of PDI-O.

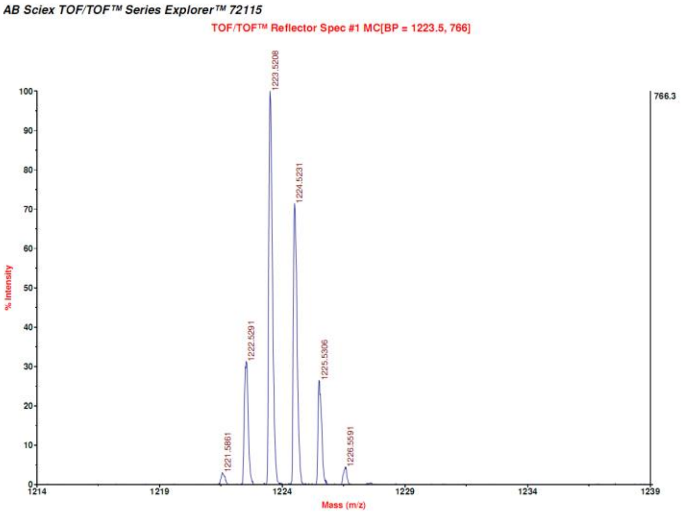

Fig. S11. MS (MALDI-TOF) mass spectrum of PDI-1S.

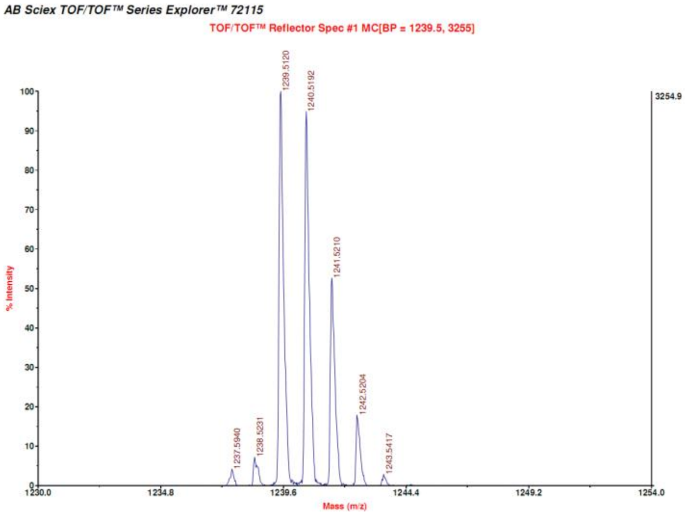

Fig. S12. MS (MALDI-TOF) mass spectrum of PDI-2S.

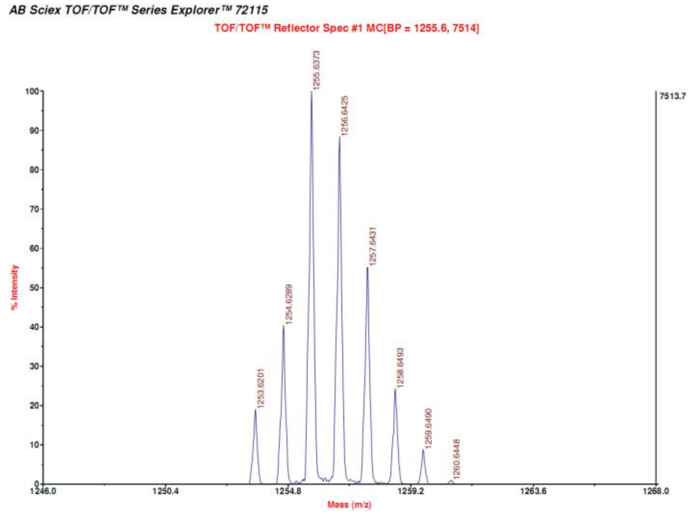

Fig. S13. MS (MALDI-TOF) mass spectrum of PDI-3S.

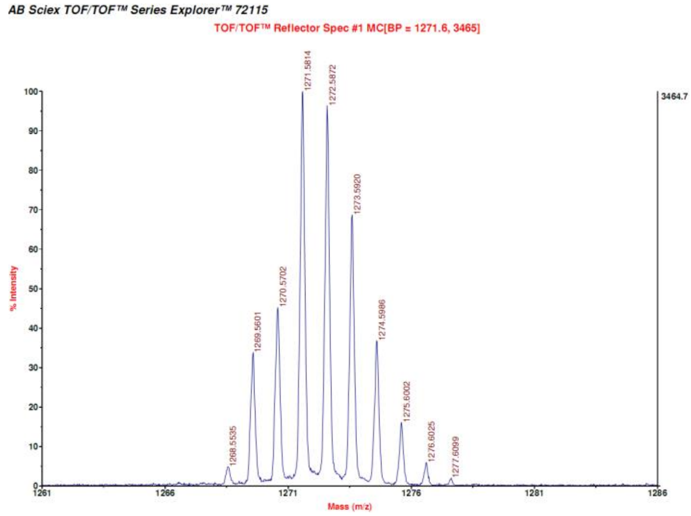

Fig. S14. MS (MALDI-TOF) mass spectrum of PDI-4S.

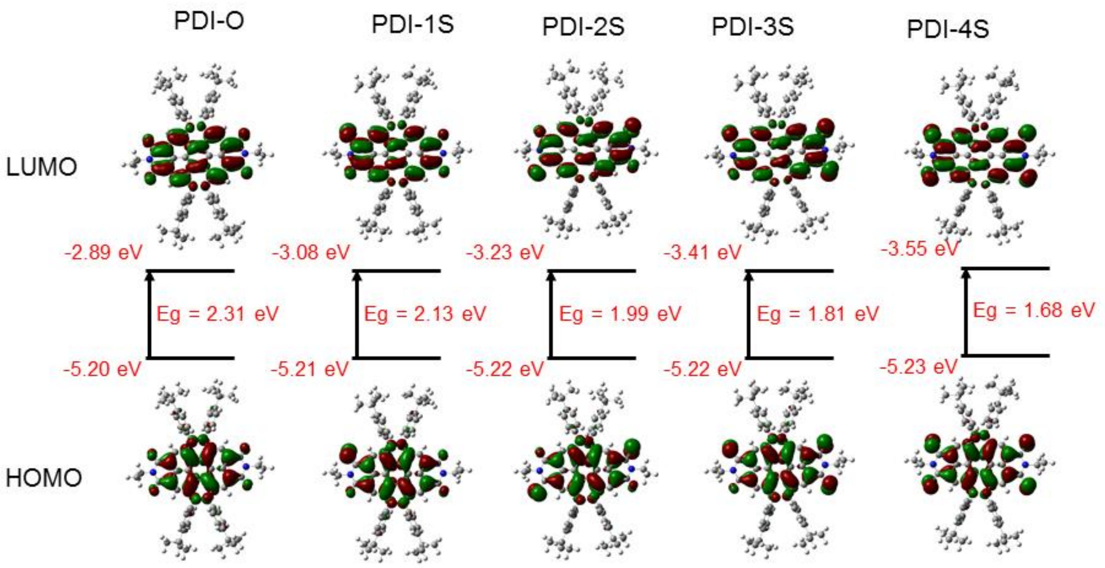

Fig. S15. Calculated HOMO and LUMO frontier orbitals for PDI-O~4S.

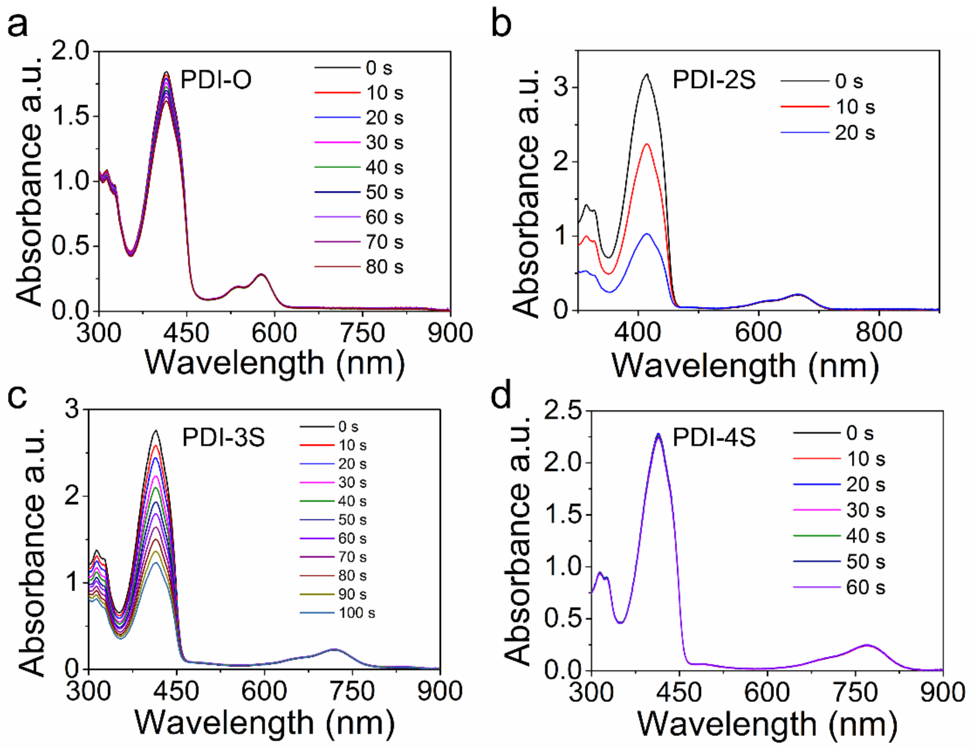

Fig. S16. Photochemical oxidation of 1,3-diphenylisobenzofuran (DPBF) by the generated $^1O_2$ from PDI-O~4S in dichloromethane (PDI-O: 550 nm green light irradiation, PDI-2S: 650 nm red light irradiation, PDI-3S: 700 nm NIR light irradiation and PDI-4S: 770 nm NIR light irradiation, 5 mW cm^{-2}).

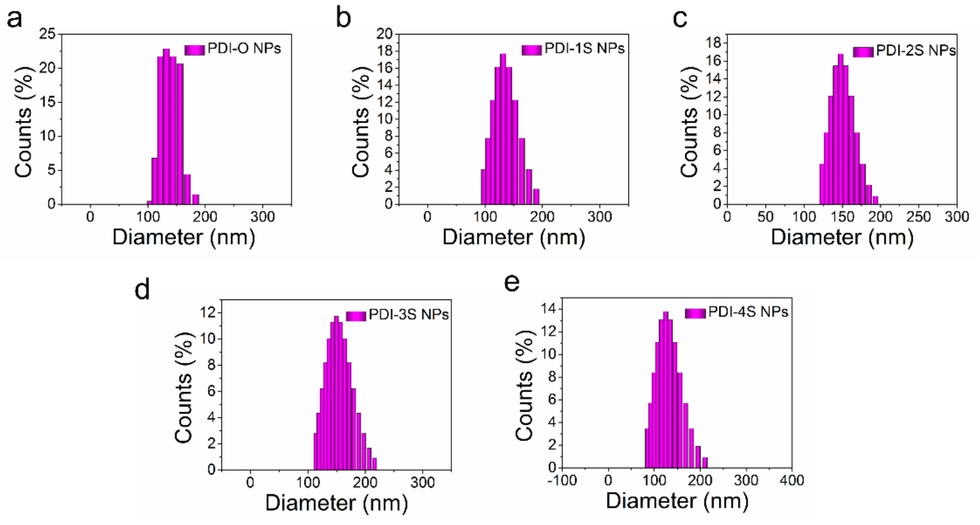

Fig. S17. (a~e) Dynamic light scattering (DLS) size profiles of PDI-O~4S NPs in deionized water.

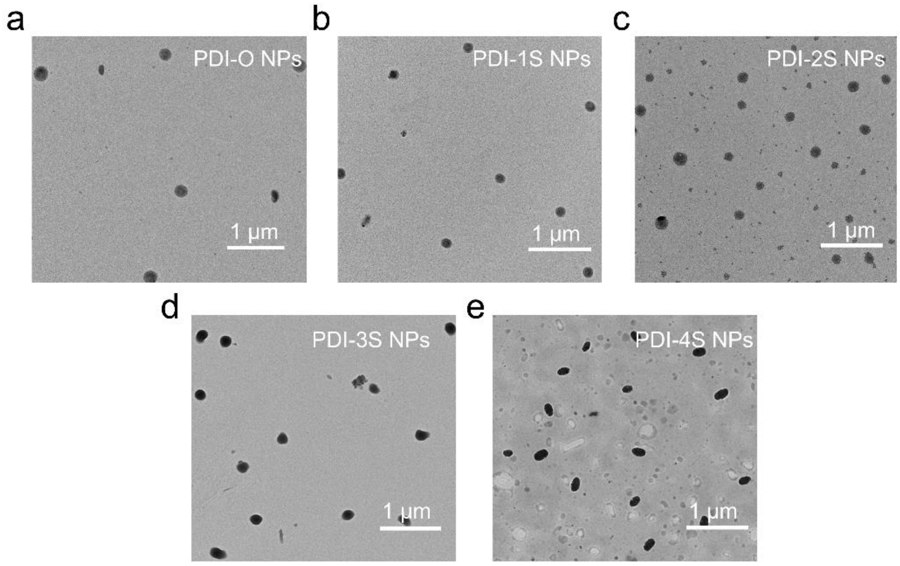

Fig. S18. TEM images of PDI-O~4S NPs.

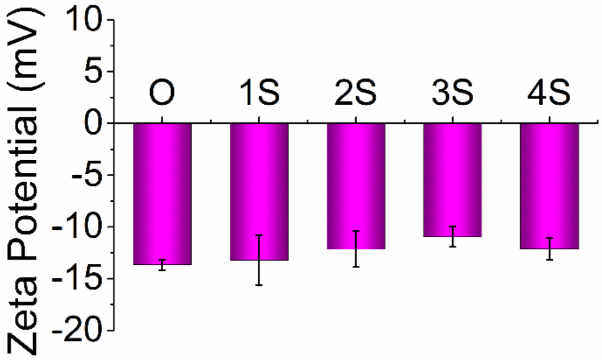

Fig. S19. Zeta potentials of PDI-O~4S NPs. Error bars, mean ± SD.

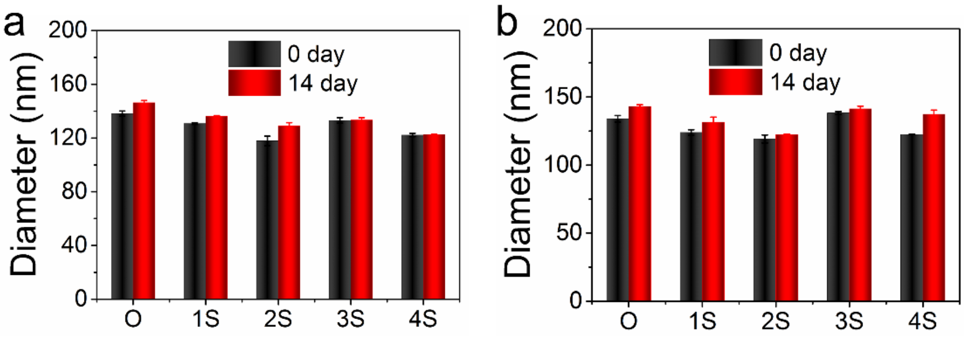

Fig. S20. The DLS size of PDI-O~4S NPs in phosphate buffer solutions (a) and DMEM (b) during storage at 4 ºC for two weeks. Error bars, mean ± SD.

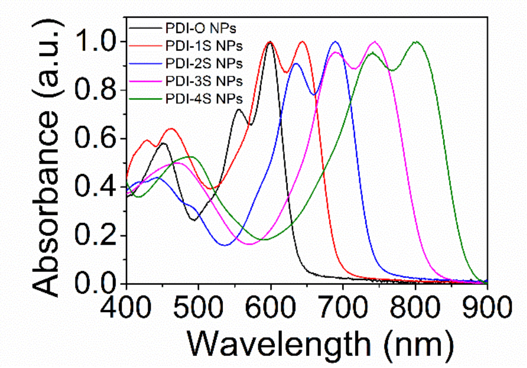

Fig. S21. Vis-NIR absorption spectrums of PDI-O~4S NPs in deionized water.

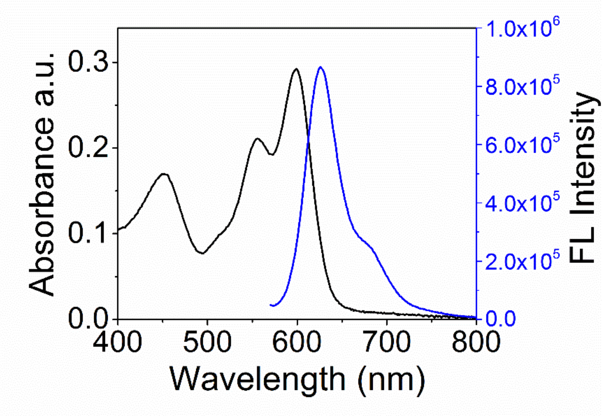

Fig. S22. Fluorescent spectra of PDI-O NPs (in deionized water, λex at the 555 nm).

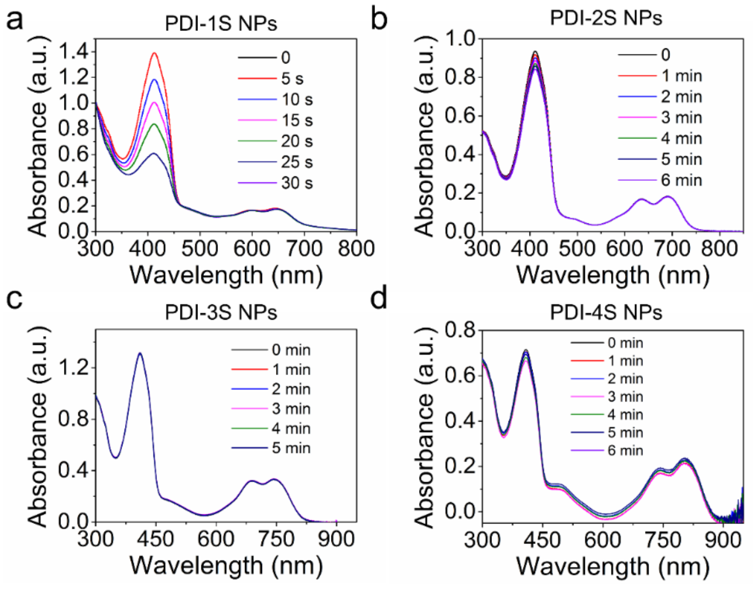

Fig. S23. Photochemical oxidation of aqueous 1,3-diphenylisobenzofuran (QDPBF) by the generated $^1O_2$ from PDI-1S~4S NPs in deionized water (PDI-1S~3S NPs: 660 nm NIR light irradiation and PDI-4S NPs: 808 nm NIR light irradiation).

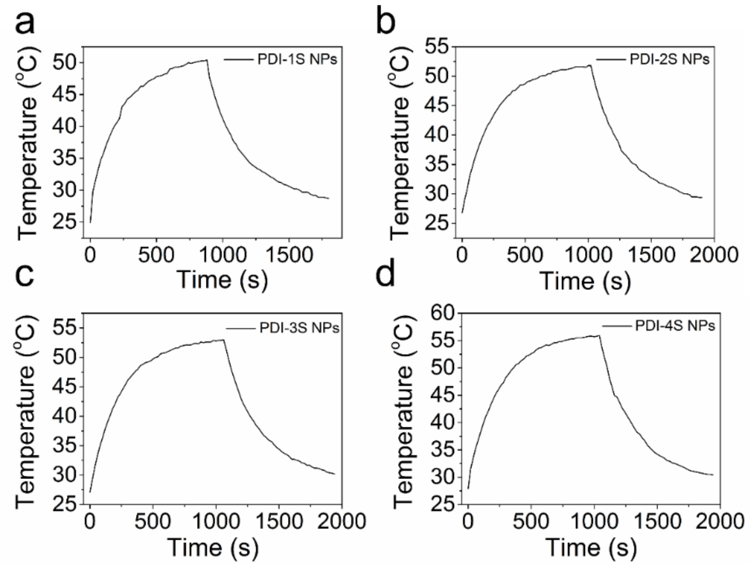

Fig. S24. Photothermal effect of PDI-1S~4S NPs in aqueous solution under laser irradiation (PDI-1S~3S NPs: $OD_{660\ nm} \approx 1$, 660 nm laser irradiation, PDI-4S NPs: $OD_{808\ nm} \approx 1$, 808 nm laser irradiation ,1 W cm^{-2}).

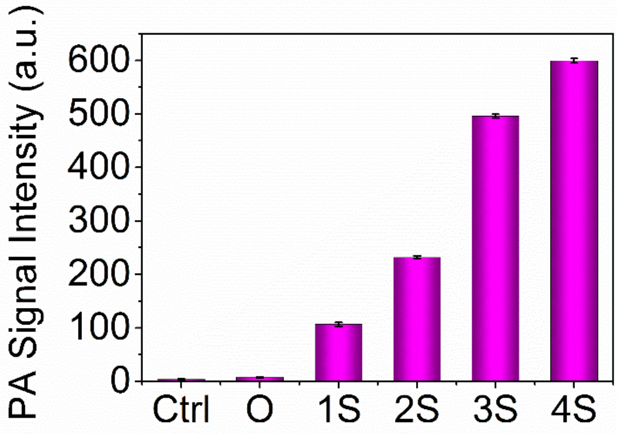

Fig. S25. Photoacoustic (PA) signal intensity of PDI-O~4S NPs (60 µM).

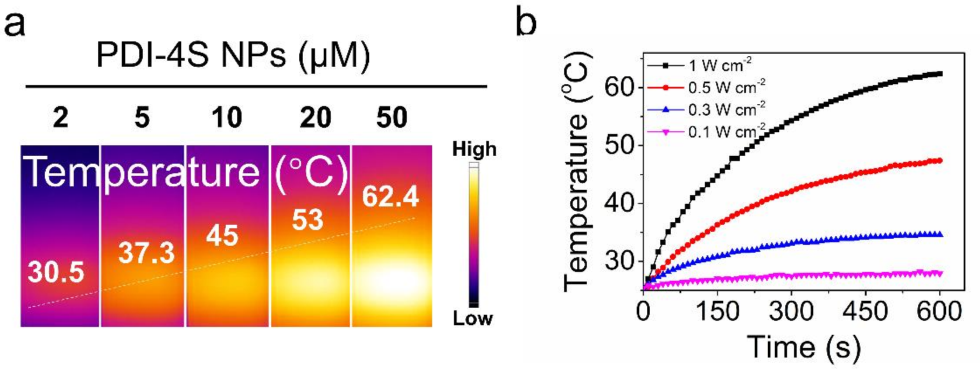

Fig. S26. (a) Infrared thermal photos of PDI-4S NPs in water irradiated by 808 nm laser light (1W cm^{-2}, 10 mins). (b) Temperature curves of PDI-4S NPs solutions (50 µM) under laser irradiation at various laser powers.

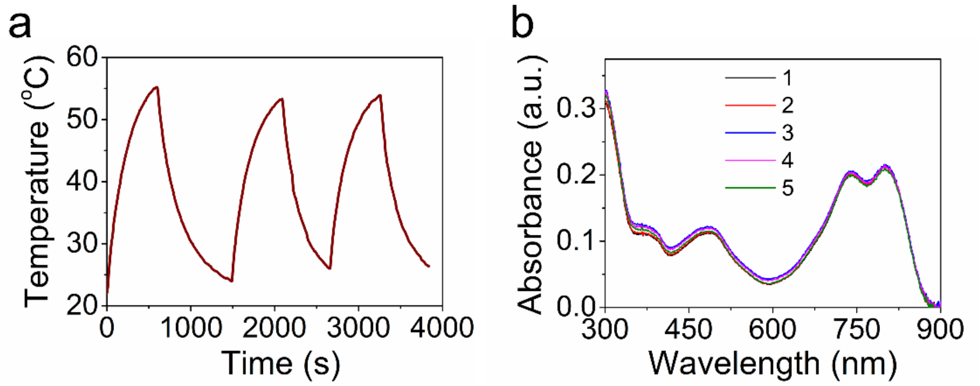

Fig. S27. (a) Photothermal stability test under 808 nm laser irradiation at 1 W cm^{-2}. (b) Photostability test under 808 nm laser irradiation at 1 W cm^{-2} for 10 min every time.

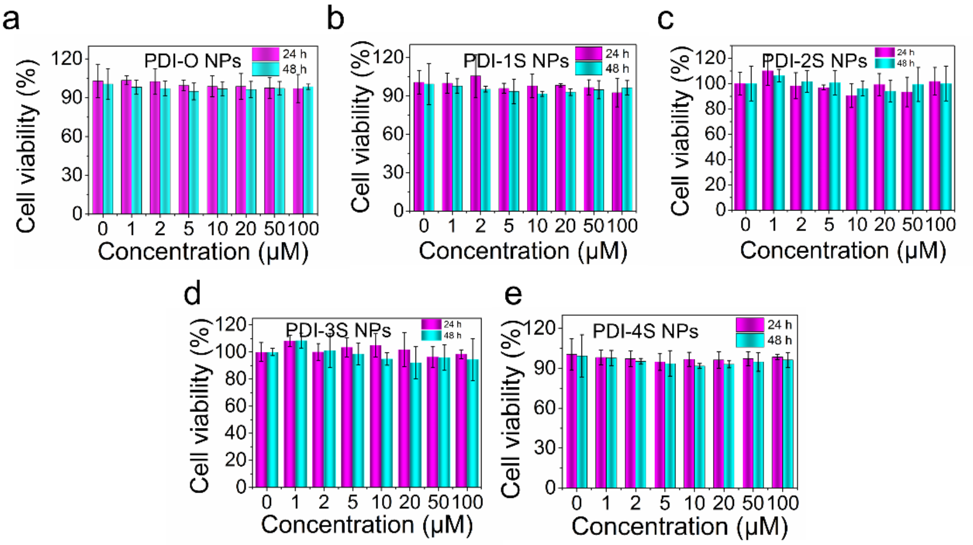

Fig. S28. Cell viability of 4T1 cells incubated with various concentrations of PDI-O NPs (a), PDI-1S NPs (b) PDI-2S NPs (c) PDI-3S NPs (d) and PDI-4S NPs (e) for 24 h and 48 h.

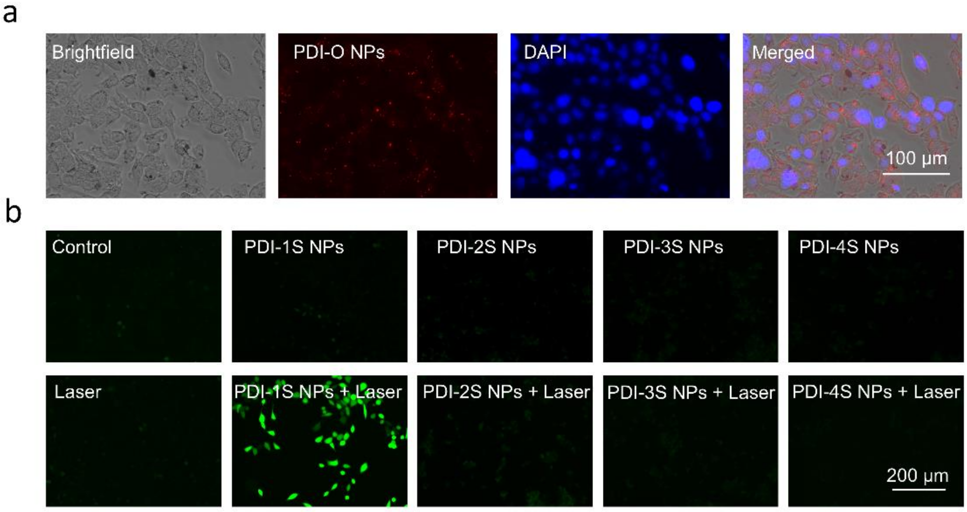

Fig. S29. (a) Fluorescence images of 4T1 cells stained with PDI-O NPs (5 μM). (b) ROS generation of 4T1 cells co-cultured with PDI-1S~4S NPs (10 μM) using dichlorofluorescein diace-tate (DCFH-DA) as a ROS probe.

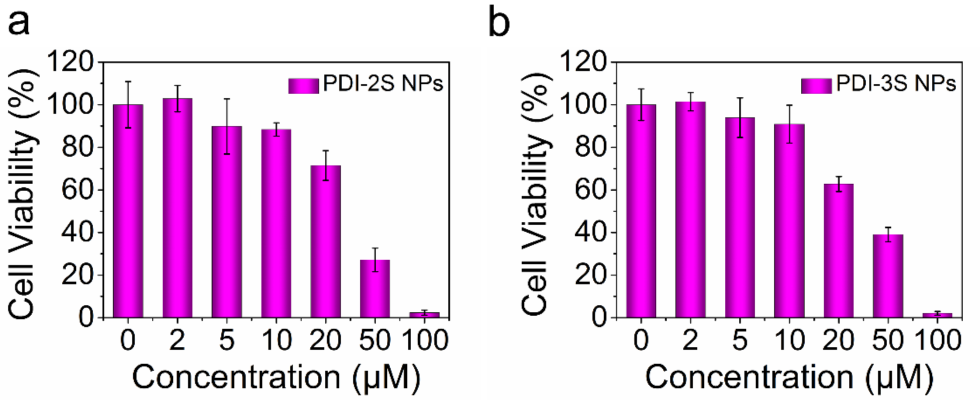

Fig. S30. Relative viabilities of cells of after laser irradiation (660 nm, 0.75 Wcm^{-2}, 5 min) with different concentrations of PDI-2S NPs (a) and PDI-3S NPs (b).

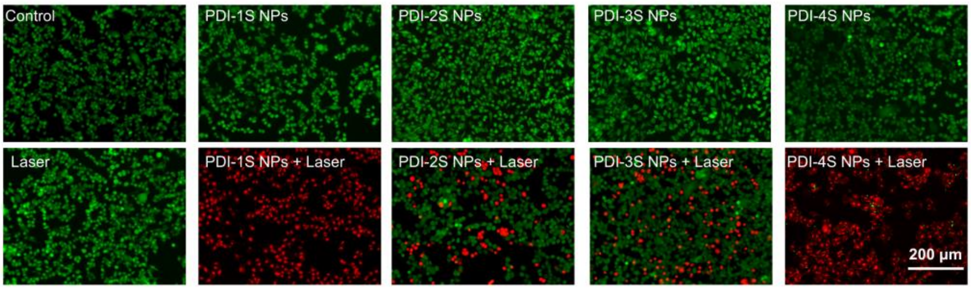

Fig. S31. The fluorescence images of 4T1 cells stained by calcein-AM/propidium iodide (PI) caused by different treatments: Control, laser, PDI-1S~4S NPs, PDI-1S~4S NPs with laser irradiation. (PDI-1S~3S NPs: 20 µM, 660 nm laser irradiation, 0.75 W/cm^{-2}, 5 min; PDI-4S NPs: 20 µM, 808 nm laser irradiation, 0.75 W/cm^{-2}, 5 min)

Table S1. Calculated electronic transition energies and ΔES_nT_m of PDI-O~4S.

Calculated electronic transition energies and ΔES_nT_m					
Energy (eV)	O	1S	2S	3S	4S
S_1	2.4212	2.2607	2.1396	1.9852	1.8666
S_2	3.2677	2.4255	2.4045	2.1078	2.0836
S_3	3.3364	3.1112	2.4102	2.3811	2.0872
T_1	0.9733	0.8204	0.6932	0.492	0.2739
T_2	2.3887	2.0398	1.8455	1.7637	1.681
T_3	2.4971	2.1266	2.1089	1.7908	1.7255
ΔES_1T_1	1.4479	1.4403	1.4464	1.4932	1.5927
ΔES_1T_2	0.0325	0.2209	0.2941	0.2215	0.1856
ΔES_1T_3	-0.0759	0.1341	0.0307	0.1944	0.1411

Table S2. Calculated spin-orbit coupling (SOC) constants between singlet and triplet states of of PDI-O~4S.

Calculated spin-orbit coupling (SOC) constants between singlet and triplet states ($\langle S_n \vert H_{SO} \vert T_m \rangle$ (Re, Im) cm^{-1})						
S	T	O	1S	2S	3S	4S
1	1	0.02	58.29673	14.42055	66.49683	85.03853
1	2	0.092736	17.71044	47.34333	3.348851	13.35027
1	3	0.438634	99.20331	11.68973	74.01697	1.781292

Table S3. The values of $[S_n|H_{SO}|T_m/E_{SnTm}]^2$ for the ISC between singlet and triplet states of PDI-O~4S.

$[S_n\|H_{SO}\|T_m/E_{SnTm}]^2(*10^6)$					
	O	1S	2S	3S	4S
$S_1 \leftrightarrow T_1$	2.94509E-06	25.28707	1.534274	30.61132	44.00274
$S_1 \leftrightarrow T_2$	0.125674705	99.21636	399.985	3.528257	79.86197
$S_1 \leftrightarrow T_3$	--	8447.164	2237.941	2237.619	2.459983
Sum	0.13	8571.668	2639.460663	2271.759	126.3247

Table S4. Photophysical properties of thionated PDIs compounds

PDIs NPs	λ_{abs} [a]/ nm	η[a]	Φ_Δ [a]/ %
PDI-1S NPs	645	27.2	58.5
PDI-2S NPs	688	30.1	0.5
PDI-3S NPs	743	32.3	< 0.1
PDI-4S NPs	803	46	< 0.1

[a]Measured in water. Singlet oxygen quantum yield (Φ_Δ) was determined with respect to MB (Φ_Δ= 52 % in aqueous solution).[9]

References:

1 C. Chen, H. Ou, R. Liu and D. Ding, *Adv. Mater.*, 2019, **32**, 1806331.

2 G. Feng, G.-Q. Zhang and D. Ding, *Chem. Soc. Rev.*, 2020, **49**, 8179-8234.

3 Z. Yang, Z. Zhang, Z. Lei, D. Wang, H. Ma and B. Z. Tang, *ACS Nano*, 2021, **15**, 7328-7339.

4 C. Ji, W. Cheng, Q. Yuan, K. Müllen and M. Yin, *Accounts of Chemical Research*, 2019, **52**, 2266-2277.

5 H. Li, L. Yue, M. Wu and F. Wu, *Colloids.Surface. B.*, 2020, **196**, 111351.

6 H. Li, Y. Zhang, B. Chen, Y. Wang, C. Teh, G. H. B. Ng, J. Meng, Z. Huang, W. Dong, M. Y. Tan, X. Sun, X. Sun, X. Li and J. Li, *ACS Appl. Bio. Mater.*, 2019, **2**, 1569-1577.

7 Q. Fan, K. Cheng, Z. Yang, R. Zhang, M. Yang, X. Hu, X. Ma, L. Bu, X. Lu, X. Xiong, W. Huang, H. Zhao and Z. Cheng, *Adv. Mater.*, 2015, **27**, 843-847.

8 J. Li, C. Liu, Y. Hu, C. Ji, S. Li and M. Yin, *Theranostics*, 2020, **10**, 166-178.

9 M. Schulze, A. Steffen and F. Würthner, *Angew. Chem. Int. Ed.*, 2015, **54**, 1570-1573.